Electromagnetic Stimulated Anisotropic Hydrogels for Guided Neuronal Morphogenesis

Bjarke Nørrehvedde Jensen[1], Tong Tong[2,3], Grith Skovborg[1], Yuge Zhang,[4] Christoph Müller[1], Cecillie Linneberg Matthiesen[1], Jens Toft Eschen[2,3], Kirstine Juul Elbæk[2,3], Yuting Wang[1], Lone Tjener Pallesen[5], Dror Seliktar[6], Mingdong Dong[4], Christian Bjerggaard Vægter[5], Anders Rosendal Korshøj[2,3], Menglin Chen[1,4]*

[1] *Department of Biological and Chemical Engineering, Aarhus University, Aarhus, Denmark*

[2] *Department of Neurosurgery, Aarhus University Hospital, Palle Juul-Jensens Boulevard 165, 11 8200 Aarhus N, Denmark*

[3] *Department of Clinical Medicine, Aarhus University, Palle Juul-Jensens Boulevard 99, 8200 13 Aarhus N, Denmark*

[4] *Interdisciplinary Nanoscience Center, Aarhus University, Aarhus, Denmark*

[5] *Department of Biomedicine, Danish Research Institute of Translational Neuroscience - DANDRITE, Nordic-EMBL Partnership for Molecular Medicine, Aarhus University, Aarhus C, Denmark*

[6] *Faculty of Biomedical Engineering, Technion – Israel Institute of Technology, Haifa 32000, Israel*

**Corresponding author: Menglin@BCE.au.dk*

Abstract

While electrical circuits are a fundamental part of neural activity, the soft microstructural extracellular environment plays a vital role in driving the morphogenesis of neurons. To leverage this, we combine a wireless electromagnetic neural stimulation system with anisotropic GelMA hydrogels to promote and guide neural morphogensis. We show that oriented GelMA hydrogels support anisotropic growth of dorsal root ganglion as potential peripheral neural guide conduit and promote the formation of hippocampal neurospheres networking along the fiber direction. The central nervous system has limited regeneration due to glial scar formation, the presence of the perineuronal network, and limited upregulation of growth-associated genes post traumatic injuries. The system was further tested on human cortical brain tissue where hydrogel microfilaments promoted neurite outgrowth in a white-matter-mimicking manner between two pieces of brain slices, opening the possibility of central neural tissue regeneration.

Keywords

Anisotropy, wireless electromagnetic stimulation, dorsal root ganglion, hippocampal neurospheres, human brain tissue

Introduction

Proper reproduction of the native extracellular matrix is imperative to ensure high neural cell viability and correct phenotypic expression. As such, the structural, chemical, and mechanical properties of the native tissue must be recreated [1]. The extracellular matrix (ECM) in both central and peripheral nervous systems is responsible for maintaining structural integrity and homeostasis. It forms the scaffolding for guiding cell migration, differentiation, and axonal outgrowth. Failure or defects in the brain ECM may result in diseases such as stroke, multiple sclerosis, Parkinson's disease, or brain injuries [1-4]. Damage to the ECM of peripheral nerves from injuries or diseases often lead to loss of function, even after undergoing autograft treatment as current "gold standard" [5-9]. Due to the difficulty in structuring hydrogels with <1 kPa modulus, limited work has been done on defined *in vitro* patterns with low modulus [10-14]. Consequently, the structures remain primitive and do not resemble physiological structures [15]. Structural morphology greatly influences cellular morphology [16, 17]. Studies have shown that, depending on the cell type, structural features as small as 33 nm and as large as 100 µm can influence cellular morphology [18, 19]. As such, nano- and microgrooves in surfaces and nano/microfibers are utilized in neural tissue engineering to align neurons and to mimic ECM structures that occur in mature nervous systems. Such anisotropic structures for neural tissue repair have been fabricated using various techniques such as electrospinning [20, 21], melt electrowriting [22-24], freeze drying [25, 26], electric fields [27], and bioprinting [28, 29]. Recently, volumetric bioprinting has emerged as an excellent method for rapid fabrication of complex 3D hydrogel structures. Based on tomography, the method utilizes several images on a rotating volume to crosslink hydrogel into a custom structure [30, 31]. Using volumetric bioprinting technology, Liu *et al.* demonstrated the rapid fabrication of filamented hydrogel [32]. The method rapidly creates highly anisotropic and aligned hydrogel microfilaments using light-based projection. The microfilaments, with diameters matching cell sizes (2-30 µm), exhibit highly unidirectional characteristics.

The electrical activity of cells plays a vital role in neural proliferation, migration, and differentiation at different stages [33]. Studies show that electrical stimulation during tissue development and regeneration can activate neural regenerative pathways resulting in cell outgrowth and migration, axonal directionality, and extension, promote neurotrophic factor production, increase neural plasticity, and cause an upregulation of regeneration-related genes [34, 35]. Delivery of direct electrical stimulation can be disruptive to the damaged tissue, can cause further damage, and has the potential risk of inducing infection both during stimulation and during the retrieval of the stimulation device [36-39]. As such wireless stimulation methods are a growing field of research

that aims to solve the limitations of direct stimulation [37]. One of the promising techniques utilizes electromagnetic induction to induce stimulating currents in materials within the damaged site.

Electromagnetic induction has been used to create a fully implantable and bioresorbable neural stimulator. A magnesium coil was coated with wolfram and encapsulated in PLGA to isolate it for implantation. Megahertz frequency magnetic fields were converted to DC-like currents through up to 15 cm of native tissue. The coil was connected to a nerve cuff for transient stimulation of the sciatic nerve of mice. Wireless electrical stimulation (monophasic, 200 µs pulse, 20 Hz frequency) was delivered to an injured nerve for 1 h per day for 1-, 3-, and 6-days post-injury. The results showed significantly increased rates and degrees of nerve regeneration in addition to increased recovery of muscle function [40, 41]. We have previously developed a highly flexible melt electrowritten neural stimulation scaffold for direct interfacing with neural cells while delivering wireless electromagnetic stimulation. The combination of anisotropic mechanical guidance and wireless electromagnetic stimulation yielded 73.2% increased neural outgrowth over 7 days of stimulation [22]. However, little focus is put into the 3D morphology of the inductive materials and as such does not utilize the combined effect of topographical guidance with electrical stimulation.

In this study, 3D anisotropic GelMA neuron guide conduit/patch was combined with wireless electromagnetic stimulation for neural cell and tissue culture in vitro (Fig. 1). The hydrogel constructs were characterized by scanning electron microscopy, swelling ratio, degradation, and mechanical modulus. Their biocompatibility and ability to guide 3D cell alignment under electromagnetic stimulation were characterized using live/dead staining and immunochemistry. Further investigation of peripheral neural guide conduit, hippocampal neurosphere formation, and white matter axonal connectivity in human brain tissue were investigated.

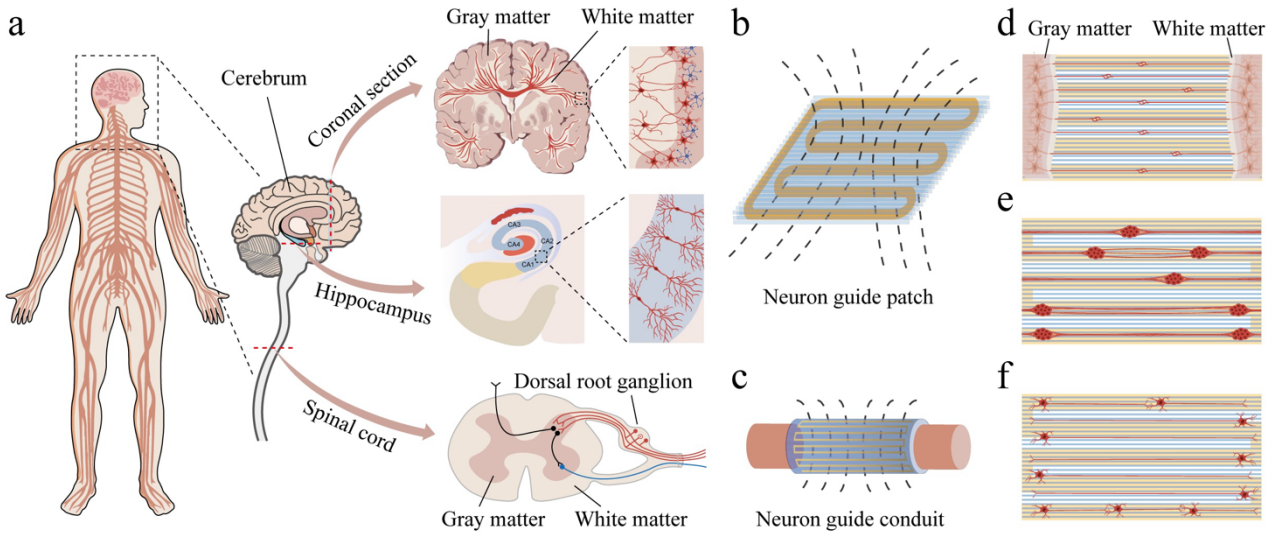

Figure 1 Oriented hydrogels with wireless electromagnetic stimulation for guided neural morphogenesis across central and peripheral nervous systems (a). Electromagnetic stimulated oriented hydrogel fibers (b,c)

guided human brain tissue white matter connectivity (d), hippocampus neurosphere formation (e) and dorsal root ganglion neural outgrowth (f).

Results and discussion

Mechanical characterization and Biocompatibility

The mechanical properties of hydrogels influence cellular processes and morphology [16]. **Figures S1a** and **S2b** illustrate bulk GelMA (GelMA-B) hydrogel and highly aligned GelMA fibrillar hydrogel (GelMA-F), respectively. The obtained GelMA-F bundles retain their structural integrity without external support while still exhibiting an exceptionally high degree of fiber alignment, as shown in FFT analysis **(Figure 2.c)**.

The swelling ratio of GelMA-B and GelMA-F hydrogels at 2%, 3%, and 4% w/v were investigated (**Figure S1c-d**). Minimal differences in swelling ratio between 2%-4% w/v GelMA is observed. However, the increased swelling ratio between GelMA-B and GelMA-F may be attributed to the void spaces created in hydrogels, which can accommodate higher amount of water between the loosely bound fibers.

The Young's modulus of three different concentrations of GelMA was measured, and it was found that the modulus increased significantly with the increase of GelMA concentration. GelMA is a temperature-sensitive hydrogel that is capable of physical crosslinking below a critical temperature [42]. It was found that the physical crosslinking of 4% w/v GelMA over 50 minutes followed by a chemical crosslinking significantly increased the storage modulus (**Figure S2e**).

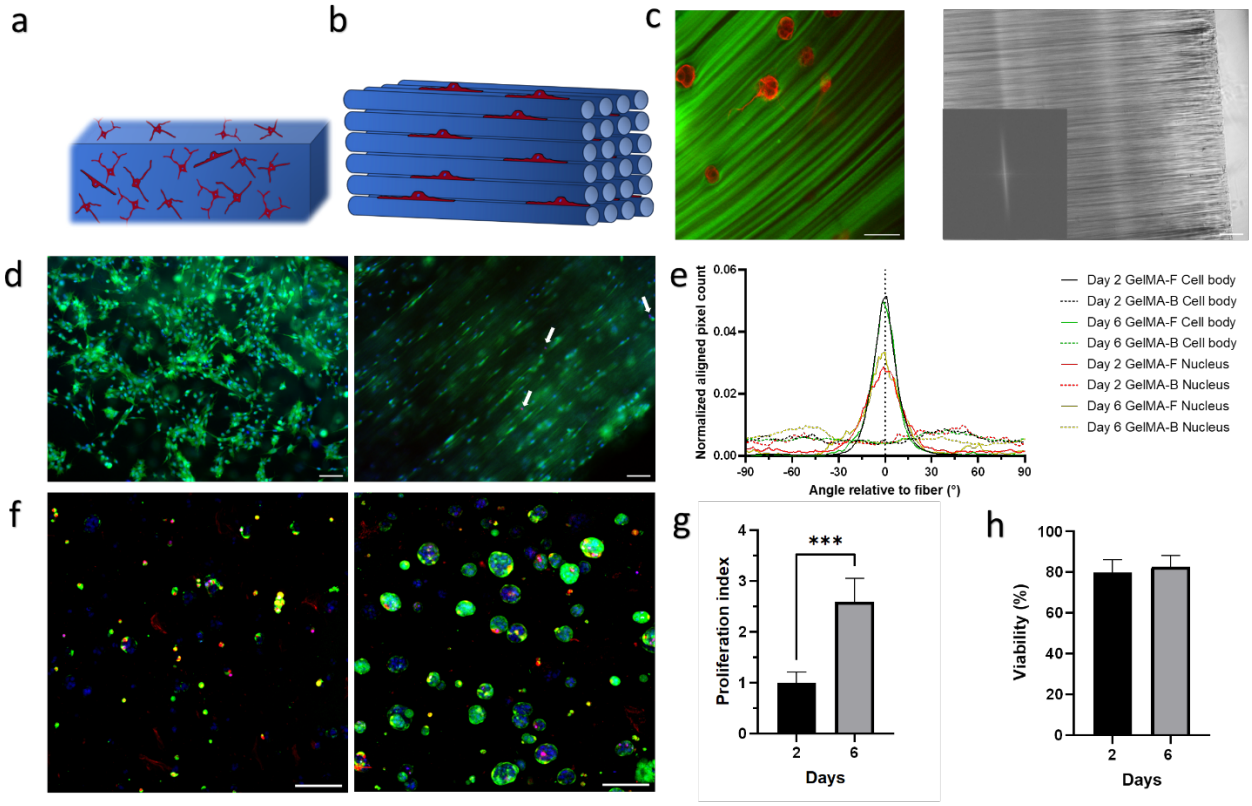

Figure 2 *Schematic of cell encapsulation in GelMA-B* ***a)*** *and GelMA-F* ***(b)****.* ***c)*** *PC12 encapsulation in FITC-GelMA-F. Scalebar = 100 µm* ***d)*** *Representative images of encapsulated eGFP-MSCs after-6 days in GelMA-B (left) and GelMA-F (right). Green = eGFP, red = propidium iodide (a white arrow indicates the few dead cells), blue = Hoechst. Scalebars* = 100 µm. ***e)*** *Directionality of eGFP-MSC nuclei and cell body after growth in GelMA-F.* ***f)*** *Representative confocal live/dead images of PC12 in 4% w/v GelMA (RT) after 2 days and 6 days in growth media. Green = calcein-AM, red = propidium iodide, blue = Hoechst. Scalebars = 100 µm.* ***g)*** *Proliferation index of PC12 cells in growth media encapsulated in 4% w/v GelMA (RT).* ***h)*** *Cell viability of PC12 cells in GelMA-F at 2 days and 6 days.*

Sculpting the 3D microenvironment during biofabrication to mimic the native tissue structure enhances the cellular differentiation process. Several structures in the body like muscles, spinal cord, and peripheral nerves possess highly anisotropic features reminiscent of fibers on which cells grow and differentiate along (**Figure 2.a-b**) [17, 43]. A neural model cell line, PC12 cells stained with *β-III*-tubulin were encapsulated in FITC-GelMA-F, showing aligned fluorescent fibers wrapping around the cells (**Figure 2.c**). Mesenchymal stem cells (eGFP-MSCs) were encapsulated and grown in the GelMA-F (**Figure 2.d**) to investigate the effect of anisotropic fibers upon the growth and spreading upon the cells. After 6 days, images show cells growing and spreading along the GelMA-F fibers. The alignment of cell bodies and nuclei along the fibers is clearly

different from cells in isotropic GelMA-B. (**Figure 2.e**). Encapsulation of undifferentiated PC12 cultured in the growth medium shows normal proliferation of 2.5 fold from day 2 to day 6 (**Figure 2.g**) and about 80% viability (**Figure 2.h**).)

Neural guide conduit for peripheral neuron repair

It is well known that neural outgrowth is guided along anisotropic structures, which is often utilized in peripheral neural regeneration [17]. (**Figure 3.a**) As shown in **Figure 3.b**, GelMA-F were successfully printed inside the electromagnetic coil made of gold-coated molten electrospun PCL coils [22]. The voltage output of the EM stimulation system was investigated with hydrogel encapsulation (**Figure 3c**). The results show a decrease (6.29 ± 0.07 folds) in the induced voltage upon GelMA encapsulation in PBS (**Figure S2.b**), where 7.2 mV is induced at 90 kHz, 10V. The GelMA in PBS functions as a conductive electrolyte thus allowing for ionic currents through the system. The conductivity of PBS is close to that of common cellular media and body fluid [44, 45].

On TCP and unstructured GelMA-B surfaces, the DRG neurons formed radially outward spreading neurites as commonly observed on isotropic surfaces [46-49]. While on the uniformly aligned GelMA-F surfaces, the neurites clearly aligned with the direction of the fibers (**Figure 3.d-e**). Furthermore, without laminin or other coatings needed for culture of DRG neurons on TCP surfaces, GelMA provides sufficient adhesion for DRG neurons for outgrowth reaching >3.2 mm over 7 days (**Figure 3.f**). β-III-tubulin and GFAP expressions were found along the same outgrowth, indicating a synergistic outgrowth between the DRG neurons and the supporting glial cells, respectively. Furthermore, synaptophysin, a typical synaptic vesicle protein, was found located along the outgrowth and soma of the DRG cells, suggesting a normal neuroendocrine function of DRG. (**Figure 3.g**).

The encapsulated PC12 cells in 2% GelMA-F were differentiated inside the neural stimulation conduit for wireless electromagnetic stimulation (**Figure 3.h**). Neurite directionality analysis of PC12 cells encapsulated in GelMA-F showed neurite outgrowth parallel to the GelMA-F fibers, independent of the stimulation (**Figure 3.i**). The wireless stimulation (8 mV, 90 kHz, 2 h/day, 7 days) significantly increased the encapsulated PC12 neurite outgrowth from 75.03 μm to 85.17 μm (**Figure 3.j**). A larger effect of wireless electromagnetic stimulation (**Figure S3)** was also observed with the encapsulation in GelMA 4% (RT) with relatively same stiffness of GelMA 2% (4 °C).

The successful fabrication of GelMA-F fiber and subsequent neurite outgrowth along the fibers indicate the promise of GelMA-F fibers for the use in nerve guide conduits for peripheral neuron repair. The ease at which tubular structures of oriented hydrogel fibers can be volumetric bioprinted within seconds and further adapted with inner channel designs makes it a promising fabrication technique for solving challenges such as nerve

misalignment, which leads to incomplete reinnervation and slows the recovery of muscle function post nerve repair [50, 51]. Potentially, a personalized nerve guide conduit may be rapidly produced within seconds to match the specific nerve bundle structure, increasing the likelihood of joining together the correct nerve fibers in a damaged nerve bundle.

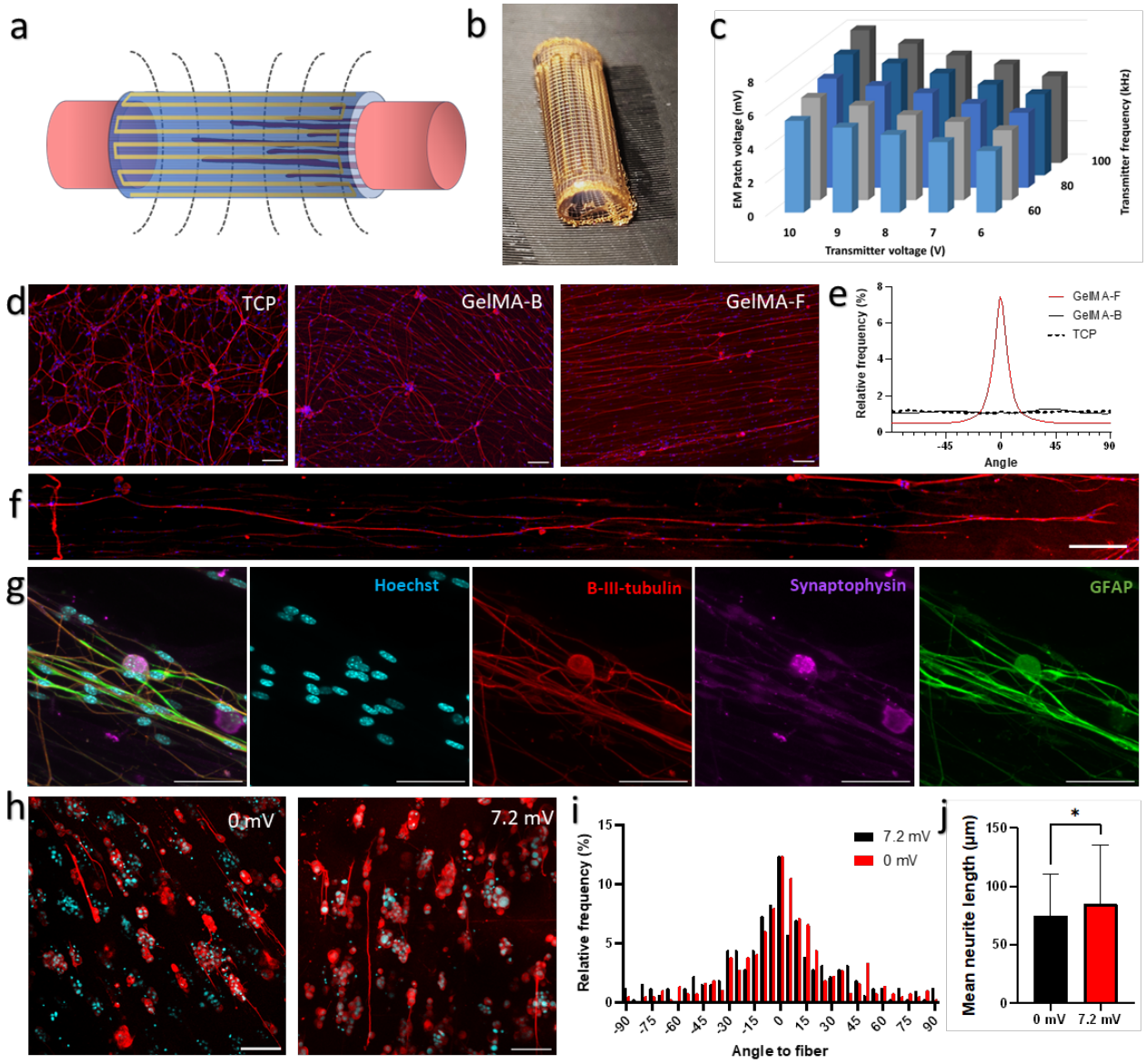

Figure 3 ***a)*** *Potential use of GelMA-F as a nerve guide conduit with wireless electromagnetic stimulation.* ***b)*** *A picture of the conduit.* ***c)*** *Voltage output ratio of EM patch 4% w/v GelMA in PBS.* ***d)*** *DRG after 7 days of culture on TCP, the surface of GelMA-B, and GelMA-F. Red = β-III-tubulin, blue/cyan = Hoechst. Scale bar 100 µm.* ***e)*** *Directionality analysis of DRG on TCP, GelMA-B, and GelMA-F after 7 days of culture.* ***f)*** *A stitched image of DRG axon after 7 days of culture. Scale bar 200 µm.* ***g)*** *Confocal images of neuronal (β-III-tubulin) and glial (GFAP) cells on 4% w/v GelMA-F after 7 days of culture. Scale bar 100 µm.* ***h)*** *PC12 cells*

encapsulated in 2% w/v GelMA-F after 7 days of NGF induced differentiation without or with wireless electromagnetic stimulated (7.2 mV, 90 kHz, 2 h/day). Red = β-III-tubulin, blue/cyan = Hoechst. Scale bar 100 µm. ***i)*** *Neurite directionality analysis of PC12 cells from* ***(h)****.* ***j)*** *Mean neurite length of PC12 cells from* ***(h).***

Hippocampal neurosphere formation

Microfluidic systems or microfabricated surfaces are widely used to guide neuronal connections to investigate basic neuronal circuits and functions [52-55]. However, while many of these systems are successful in generating circuits, they often lack the potential influence of the mechanical and molecular properties of the surrounding ECM. As an extension of the cerebral cortex situated deep into the temporal lobe, the hippocampus is vital for learning, memory, and spatial navigation. It is vulnerable to a variety of stimuli and hence is important clinically both diagnostically and therapeutically for cognitive decline and diagnosis of Alzheimer's disease. Intriguingly, the hippocampus is one of the unique regions in brain where the neurogenesis [56] continues even in adult life. Here we investigate if GelMA-F can be used as a step towards a platform for generating guided hippocampal neurospheres by utilizing the aligned surface topography of GelMA-F. Furthermore, we investigate if the mechanical property of hydrogel influences the morphology and growth patterns of hippocampal neurons.

Hippocampal neurons were seeded onto laminin-coated tissue culture plastic (TCP), 4% w/v GelMA-F and 8% w/v GelMA-F. On TCP, hippocampal neurons appeared as singular cells with neurites spreading radially outward (**Figure 4.a,d-e**). The neurites, rather than spreading radially outwards from the neurospheres, were observed to form axon bundles on GelMA-F (**Figure 4.b-c**). No significant difference in axon bundle widths was observed between 4% and 8% GelMA-F (**Figure 4.f**). Minimal clustering was observed on TCP while a significant increase in the cluster size was observed on GelMA-F 4% compared to TCP (**Figure 4.g**). Hippocampal neuron clustering has been observed in literature, often initiated by changes in surface properties such as surface contact angle [57] or surface coating chemistry [58, 59]. Previously, a gelatin nanofiber network fabricated by Tang *et al.* did not result in the formation of neurospheres but rather an individual cell distribution [60]. On the other hand, Bansal *et al* observed clustering of hippocampal neurons on their GelMA coated microelectrodes [61]. Hörberg *et al* observed neurosphere formation on their polyethylenimine-coated electrodes and found that the ratio of astrocytes and neurons influenced the neurosphere size [62]. It is thus the first time that GelMA-F microfiber pattern has been shown to induce hippocampal cell clustering, forming neurospheres.

The cell and neurite directionality in relation to the direction of GelMA-F fibers was analyzed (**Figure 4.h**), where a clear directionality was found on GelMA-F with many more matured neurons compared to TCP, especially more aligned neurons and axons were found along the 4% GelMA-F, forming a solid axon network among neurospheres. Interestingly, while thick axon bundles were observed between neurospheres along the

GelMA-F fibers, axon bundles were observed much thinner crossing between neurospheres across the GelMA-F fibers, suggesting swifter transmission in the direction aligned with the fibers.

The GelMA-F provides a straightforward platform for generating hippocampal neurospheres on a topographically controlled soft hydrogel surface. Furthermore, the use of a hydrogel system enables the ease of control of the biologically relevant mechanical properties, a feature that is uncommon in currently available systems [63-65]. Therefore, the GelMA-F enables facile establishment of neurospheres or organoids as in vitro brain models to study cognitive diseases diagnostically and therapeutically.

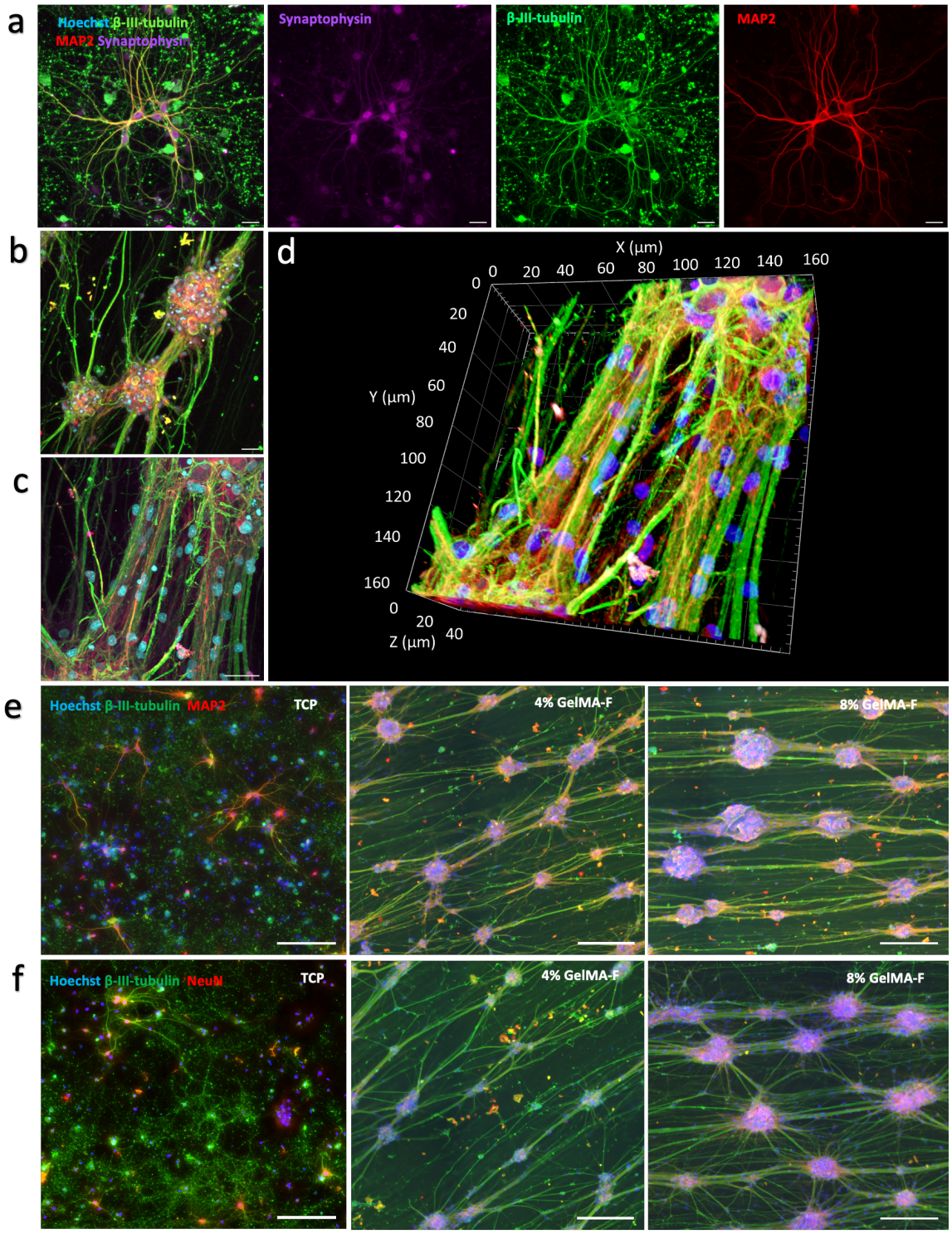
a
Hoechst β-III-tubulin
MAP2 Synaptophysin
Synaptophysin
β-III-tubulin
MAP2
b
c
d
X (µm)
Y (µm)
Z (µm)
e
Hoechst β-III-tubulin MAP2
TCP
4% GelMA-F
8% GelMA-F
f
Hoechst β-III-tubulin NeuN
TCP
4% GelMA-F
8% GelMA-F
g
Relative frequency (%)
Axon width (µm)
TCP
4% GelMA-F
8% GelMA-F
h
Relative frequency (%)
Cluster size (µm²)
TCP
4% GelMA-F
8% GelMA-F
i
Relative frequency (%)
Angle to FLight fibers (°)
TCP
4% GelMA-F
8% GelMA-F

Figure 4 ***a-c)*** *Confocal images of hippocampal neurons on TCP* ***(a)*** *and 8% w/v GelMA-F* ***(b-c)*** *after 14 days of culture (DIV). Scale bar 25 µm.* ***d)*** *3D reconstruction of DRG axon bundles in (c)****. e-f)*** *Hippocampal neurons on TCP, 4% w/v GelMA-F, and 8% w/v GelMA-F after 14 days of culture (DIV). Scalebar 200 µm.* ***g)*** *Relative frequency distribution of axon bundles widths.* ***h****) Cluster size distribution of neurospheres formed on 4% w/v GelMA-F and TCP.* ***i)*** *Cluster and axon angle distribution in relation to direction of GelMA-F fiber direction.*

Connectivity in the white matter of human cortical brain tissue

Anisotropic features are found throughout the white matter of the brain. [66] The main function of the white matter is to connect neurons from different brain regions to each other by myelinated axons. The white color comes from the abundant presence of lipids in the myelin sheaths made by oligodendrocytes. The highly ordered axonal structure underlies white matter functionality and plays a major role in brain connectivity. The oriented gelatin hydrogel fibers are a potential platform for recreating these vital brain structures in damaged tissue.

Human brain tissues from the cortex region infiltrated with glioblastoma cancer were placed on GelMA-F to investigate outgrowth guidance. A slice of brain tissue was cut in two pieces which were placed onto the gel with a gap of 1-1.5 mm (**Figure 5.a**). Specifically, they were placed on top of GelMA-F (2% w/v) with gray/white matter orientation perpendicular to the fiber direction, investigating the role of GelMA-F on the topographical guidance of the axonal pathways transitioning from the gray matter into the white matter. Highly aligned neural outgrowth was observed from the brain tissue edge following the direction of the GelMA-F fibers, mimicking white matter axonal structure (**Figure 5.d-e**), as compared to the random outgrowth on GelMA-B (**Figure S4.a-b**). Cell migration from the tissue edge along the GelMA-F fibers was observed indicating that the GelMA-F fibers are permissive for both neural outgrowth and cell migration. The angle between the tissue edge and direction of GelMA-F fiber was found to significantly influence the axonal outgrowth in the white matter (**Figure 5.h-i**). A clear decline in the number of outgrowths was observed as the angle increased, with no outgrowth above an angle of 75 degrees, confirming an evident topographical effect of GelMA-F on axonal outgrowth in white matter. After 21 days, the highly aligned (**Figure 5.j**) outgrowth on GelMA-F (**Figure 5.e)** nearly had the gap sealed. On the other hand, certain connectivity with holes was generated on the membrane insert without GelMA-F (**Figure 5.c**), where axonal growth cones highly interacted with surrounding glial cells (**Figure 5.b-c**).

Glial Fibrillary Acidic Protein (GFAP) is a major protein found in the astrocytic cells of the brain, and it is considered a marker of astrogliosis, following CNS injuries and neurodegeneration, as in multiple sclerosis and Alzheimer's disease, and malignancies of glial origin, glioblastoma. GFAP is a key intermediate filament protein of glial cells involved in cytoskeleton remodeling and linked to tumor progression. Remarkably, further post-staining with GFAP shows very limited presence of GFAP on GelMA-F outgrowth but GFAP-positive glial cell outgrowth on membrane well-inserts (**Figure S5 and Figure 5.f-g**), suggesting GelMA-F selectively induced neurite outgrowth rather than glioblastoma microtubes associated with tumor progression.

Upon 7 days EM stimulation (7.2 mV, 90 kHz, 2 h/day, 7 days), massive outgrowth of human brain tissue onto the EM stimulation patch was observed (**Figure 5.k**). Furthermore, cell migration is seen onto the wall of the

EM stimulation patch (**Figure 5.l**), where both the nucleus and cell body appear to follow the direction of the anisotropic topographical features of the EM coil.

Therefore, GelMA-F guided neural outgrowth of human brain cortical tissue, demonstrating their potential use for expanding our understanding on how glial cells interact with axonal growth throughout neurodevelopment and investigating growth patterns of axonal connectivity in white matter of healthy and cancerous human brain tissue for physiological/pathological modeling. Strikingly, GelMA-F appeared non-permissive for GFAP positive glial microtube outgrowth. At this stage we can only offer some hypotheses that might explain this intriguing finding, considering the limitations of our technique. The GelMA fibers show characteristics of radial glial fibers which are known to act as a scaffold for postnatal ventricular-subventricular zone (V-SVZ)-derived neuroblasts that migrate to the lesion site to promote neuronal regeneration. White matter maturation is a complex process combining changes in axonal diameter and packing, myelin thickness, and composition. The role of gray matter in modulating cortical activity through topographically guided white matter is not investigated in our study.

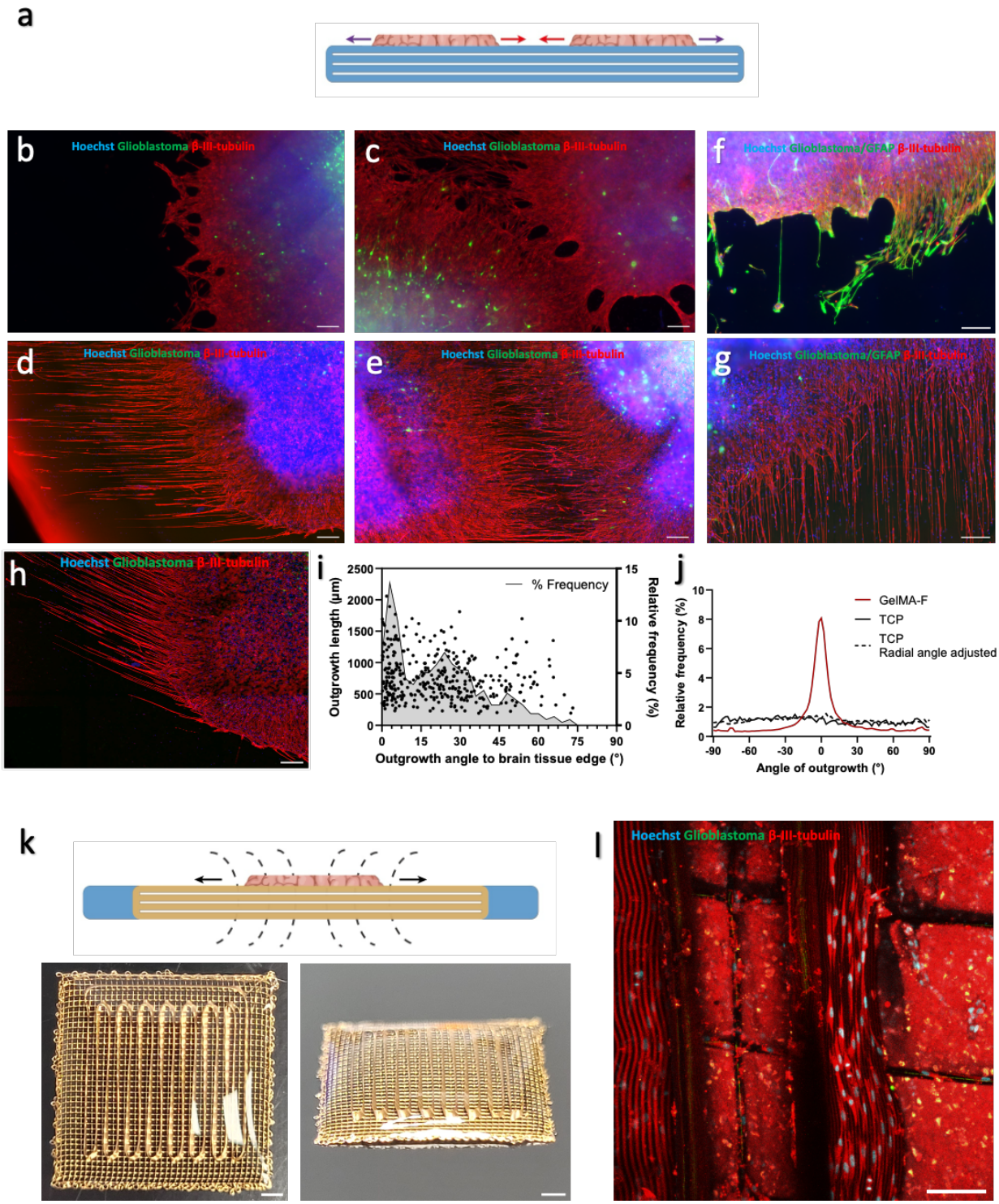

Figure 5 a) *Outgrowth from slices of human cortex brain tissue after 21 days on* ***b-c)*** *membrane well-insert (****b*** *– side,* ***c*** *- middle), and* ***d-e)*** *2% w/v GelMA-F (****d*** *– side,* ***e*** *- middle). Blue = Hoechst, red = β-III-tubulin, green = glioblastoma. Outgrowth from slices of human cortex brain tissue after 21 days post-ICC-stained with GFAP on* ***f)*** *membrane well-insert, and* ***g)*** *2% w/v GelMA-F. Blue = Hoechst, red = β-III-tubulin, green = glioblastoma/GFAP. Scalebar = 200 µm.* ***h)*** *Adjusted angle of* ***d)*** *demonstrating the effect of the angle between*

the tissue and GelMA-F on the number and length of neural outgrowth. Blue = Hoechst, red = β-III-tubulin, green = glioblastoma. Scalebar = 200 µm. ***i)*** *Neural outgrowth length against outgrowth angle to brain tissue edge.* ***j)*** *Directionality analysis of neural outgrowth from human cortex brain tissue.* ***k)*** *Schematic and photographs of EM patch and cell migration* ***(l)*** *from brain tissue onto stimulation interface of the EM patch.*

Conclusions

In summary, we discovered a few intriguing topographical effects of the anisotropic hydrogel fibers on neural cell and tissue cultures in vitro, spanning from peripheral neural guide conduit and hippocampal neurosphere formation to white matter axonal connectivity of human brain cortex tissues. Further wireless EM stimulation was found to increase neural outgrowth of peripheral neurons while supporting neural outgrowth of brain cortex tissue. Facile establishment of hippocampal neurospheres or organoids as in vitro brain models paved the way to study cognitive diseases diagnostically and therapeutically. Intriguingly, the oriented GelMA hydrogel fibers selectively induced neurite outgrowth rather than glioblastoma microtubes associated with tumor progression, opening new possibilities for CNS regeneration.

Methods and materials

Materials and fabrication of the electromagnetic stimulation patch

The fabrication of the EM receiver coil follows the procedure described in our previous paper with minor alterations [22]. Polycaprolactone (PCL) was used as raw material and was electrowritten without any modifications (medical grade, PURESORB PC 08 PCL, Corbion). The PCL receiver coil on PCL support grids were electrowritten using a melt electrowriting instrument (CAT000111, Spraybase, Ireland). The structure was designed and written in G-code which was run by a Mach3 motion control software. PCL was melted at 80 °C for one hour before printing through a stainless-steel needle (24 G). A 10 cm diameter Silicon-wafer was used as a collector at a 4 mm distance from the needle. A 4.25-4.5 kV high voltage was applied between the needle and the collecting plate. A flow rate of 0.55 bar was controlled by a Spraybase® Pressure Driven System. The coil (EM receiver) was printed at a rate of 1000-1050 mm min^{-1} with a support grid at a rate of 75 mm min^{-1}. The coil structure and support grid were printed with 40 layers and 2 layers, respectively. The G-code used for melt electrowriting of the anisotropic neural stimulation patch can be found in Supplementary Table 1. The resulting patch was subsequently coated with 4 nm titanium and 80 nm of gold using E-beam GLAD (Cryofox Explorer 500 GLAD). During coating the scaffolds were tilted 20 degrees and rotated at 3 rpm.

The wireless EM stimulation system used for stimulating neural cell growth is comprised of a receiver coil patch placed in a 24-well plate and a rectangular transmitter coil placed around the well plate. The transmitter coil size is matched to fit around a standard well plate to minimize the distance between the patch and the transmitter coil. The transmitter coil was made of 100 turns of copper wire (11 cm x 15 cm) connected to a Waveform Generator (HP 33120A, Hewlett Packard) supplying alternating current. The voltage and frequency applied through the transmitter coil were adjusted to produce the desired voltage output in the receiver coil scaffold.

GelMA synthesis

Gelatin type A from porcine skin was dissolved at 10% w/v in PBS buffer pH 7.2 (Gibco) at 60 °C under stirring overnight. Methacrylic anhydride (MA) was added dropwise at a rate of 0.5 mL/min to a final MA concentration of 10% v/v using a syringe pump under vigorous stirring. The GelMA solution was allowed to react for 3 hours at 50 °C under stirring. The GelMA solution was diluted with PBS pH 7.2 to one-fifth the concentration under stirring and subsequently transferred to dialysis tubes and dialyzed against 10x volume distilled water at 50 °C for 7 days with water changes every day. The dialyzed GelMA solution was freeze dried for 7 days and stored at -20 °C until use.

Material characterization

The voltage output of the receiver coil was recorded by an Agilent DSOX3012A oscilloscope.

The compression stress-strain measurements of GelMA were performed by compression of cylinders (Ø=8.4 mm, L=20 mm) of freshly prepared 2%, 3%, and 4% w/v GelMA using a BOSE Electroforce 3200 (BOSE). The cylinders were compressed at a rate of 1 mm/s with a force resolution of 0.1g.

The dynamic rheological measurements of GelMA were performed using a Discovery HR20 rheometer with temperature control and with a custom-built glass stage for delivery of 405 nm light for photo crosslinking of the sample during measurements. Liquid GelMA precursor (200 µL, 37 °C) with 1 mg/ml LAP was deposited on the measurement stage (Ø10mm, 600 µm gap, 37 °C). The measurements were initiated immediately with the applied frequency (6.24 rads/s) and stain (1%) within the linear force range. The photo polymerization was initiated at the timepoint indicated in the results.

Preparation of projection images for biofabrication

The biofabrication projection images were created with Inkscape, and their dimensions were set to a fixed resolution of 1024 x 768 pixels. The images were in 8-bit greyscale, where completely white pixels represented full light projection. The width of each pixel was set by the system to approximately 27 µm. The files can be found in the supplementary information.

GelMA-B and GelMA-F biofabrication

To prepare GelMA precursor, freeze dried GelMA was dissolved in PBS at 37 °C to the desired concentration. A stock solution of LAP (50 mg ml^{-1}) was added to achieve a final concentration of 1 mg ml^{-1} LAP. The GelMA precursor was filtered by a 0.2 µm filter before use to sterilize and remove particles. For encapsulation of PC12 cells and eGFP-MSC cells in GelMA-B and GelMA-F, PC12 cells and eGFP-MSC cells were resuspended in GelMA precursor before light exposure at a cell density of 1 x 10^6 cells ml^{-1} or 0.4 x 10^6 cells ml^{-1}, respectively.

To fabricate GelMA-F structures, the GelMA precursor was transferred to sterile glass vials (Ø = 1.5 cm) and was thermally crosslinked in a 4 °C water bath for 30 minutes. The image projections were performed using a tomographic volumetric printer (Tomolite version 2.0 Performance-closed, Readily3D SA). The light intensity was set to 10.5 mW cm^{-2}. The photo-crosslinked GelMA was post projection reheated to 37 °C in a water bath and the structure was retrieved with a sterile spatula. Non-crosslinked GelMA washed away with PBS and replaced with warm growth media for cell laden structures.

For PC12 cells seeded into rolled neural stimulation patches with GelMA-F, the protocol was slightly altered. The neural stimulation patch was first rolled and slid into 1 cm long silicone rubber tuber (Ø = 3400 µm), UV sterilized for 60 minutes. The bioresin was injected into the silicone rubber tube, transferred to the printing vial, and exposed to the desired projection image. The crosslinked coil-GelMA-F structure was gently removed from the silicone tube with a sterile metal stick (Ø= 3mm), rinsed with PBS, and transferred to culture media.

To fabricate GelMA-B, the same method as described above was used utilizing a 365 nm UV lamp (6W, VL-6.L, Vilber Lourmat) to photo-crosslink the GelMA precursor.

eGFP-MSC Cell culture

eGFP-MSC cells were precultured in a T75 culture flask (Sarstedt) in growth medium (10% fetal bovine serum (FBS), 1% penicillin-streptomycin (P/S) in high glucose DMEM (Gibco)). Prior to GelMA-B and GelMA-F biofabrication, eGFP-MSC cells in a T75 culture flask at ~80% confluency was rinsed twice with prewarmed PBS (37 °C), and trypsinized with 0.05% Trypsin-EDTA (Gibco) for 5 minutes at 37 °C. The trypsination was inhibited with twice the volume of growth medium and centrifuged for 5 minutes at 250g. The cells were resuspended in fresh growth medium or GelMA precursor and further used as described in the GelMA-B and GelMA-F biofabrication method section. Growth media was fully changed every 2-3 days.

PC12 Cell culture

PC12 cells were prepared and cultured similarly to previous work [23, 24]. A collagen IV coated T25 culture flask (Sarstedt) was used to preculture PC12 cells (ATCC® CRL-1721™) in growth medium (15% horse serum (HS), 2.5% fetal bovine serum (FBS), 1% penicillin-streptomycin (P/S) and 0.5% HEPES buffer

in DMEM/F12 Glutamax). Prior to GelMA-B and GelMA-F biofabrication, PC12 cells in a T25 culture flask at ~80% confluency were rinsed twice with prewarmed PBS (37 °C), and trypsinized with 0.05% Trypsin-EDTA (Gibco) for 5 minutes at 37 °C. The trypsination was inhibited with twice the volume of growth medium and centrifuged for 5 minutes at 250g. The cells were resuspended in fresh growth medium or GelMA precursor and further used as described in the GelMA-B and GelMA-F biofabrication method section.

The cells-laden hydrogel/patch structures were cultured in the growth medium for 1 day after which the media was changed to PC12 cell differentiation medium (0.5% HS, 0.5% FBS, 1% P/S and 50 ng ml^{-1} of nerve growth factor (NGF, 2.5S, Gibco) in DMEM/F12 Glutamax (Gibco). The first day of stimulation was initiated 1 day after transferring into differentiation media. The cells were stimulated for 2 hours per day throughout the differentiation period. For clarity, the voltage and frequency are stated in the result section of each experiment. PC12 Differentiation media was replenished every second day post stimulation.

All patches were UV sterilized (254 nm) for 2 × 30 minutes in 24-well plates before use.

DRG cells culture

Neuronal-enriched DRG cultures were prepared as previously described with the following modifications [67]. Postnatal day 1-4 C57BL/6J mice from Janvier lab were euthanized, disinfected in 70 % ethanol and 40 DRGs from each mouse were dissected and pooled into ice-cold HBSS medium (STEMCELL Technologies, cat. No. 37150). The DRGs from 4 pups were digested for 30 min at 37°C using 13.33 U/ml papain (Worthington, cat. No. LS003126). The DRGs were then centrifuged for 1 min at 500g, papain was aspirated, and they were further digested for 30 min in 4 mg/ml collagenase II (Worthington, cat. No. LS004176) and 4.66 mg/ml dispase II (Sigma-Aldrich, cat. No. D4693) at 37°C. The digested tissue was centrifuged for 1 min at 500g and the collagenase/dispase solution was aspirated. The cells were washed in DMEM (Gibco, cat. No. 41965-039) with 10 % (v/v) FBS (Sigma-Aldrich, cat. No. F9665) and 1 % (v/v) pen/strep (Sigma-Aldrich, cat. No. P4333), centrifuged for 1 min at 500 xg and manually triturated using a p1000 pipette in the same buffer with 40 Kunitz units Deoxyribonuclease I (Sigma-Aldrich, cat. No. DN25-1G). Debris was removed from the cell suspension by filtering through a 100 µm cell strainer (Falcon, cat. No. 352360). Dissociated cells were pre-seated on non-coated plates for 1.5 hours at 37°C. Neuron-enriched cells were harvested, centrifuged for 1 min at 500g and resuspended in DRG culture media (DMEM with 10 % (v/v) FBS, 1 % (v/v) pen/strep, 25 ng/ml neurotrophin-3 (NT-3, Alomone Labs, N260), and 25 ng/ml nerve growth factor (NGF, 2.5S, Gibco, 13257-019)). The cell suspension was then seeded onto 4% w/v GelMA-B or GelMA-F, or onto poly-d-lysin+laminin coated TCP at a seeding density of 50×10^3 cells/cm^2. The DRG cells were maintained in a humidified atmosphere at 37°C and 5% CO_2 in DRG growth medium for 7 days in vitro (DIV). Half the volume of growth medium was replaced with fresh DRG growth medium every 2 days.

Hippocampal neuron cell culture

Dissociated rat hippocampal neuron cultures were prepared and maintained as previously described [68]. Briefly, rat hippocampi were dissected from postnatal day 0 to 1 pups of either sex (Sprague-Dawley strain; Charles River Laboratories), dissociated with papain (Sigma-Aldrich), and then seeded at a density of 40×10^3 cells/cm^2 onto 4-8% w/v GelMA-F or poly-d-lysine–coated tissue culture plates (SARSTEDT). Neurons were maintained in a humidified atmosphere at 37°C and 5% CO_2 in hippocampal growth medium (Neurobasal-A supplemented with B27 and GlutaMAX-I; Life Technologies) for 21 days in vitro (DIV). Half the volume of hippocampal growth medium was replaced with fresh hippocampal growth medium twice per week.

Glioblastoma tissue acquisition

The glioblastoma tissue acquisition followed the procedure described in our previous work [69]. All procedures with human tissue and data were approved by and conducted in accordance with the Scientific Ethics Committee for the Region of Midtjylland Denmark (official name in Danish: De Videnskabsetiske Komitéer for Region Midtjylland) (journal number: 1-10-72-82-17) and conducted in accordance with the ethical principles of the World Medical Association Declaration of Helsinki [70]. Surgical specimens were collected at the neurosurgical department at Aarhus University Hospital (Denmark) through collaboration with local surgeons. Before participating in the study, all patients gave informed consent for the donation of tissue. The patients included in the study were undergoing surgery for GBM, and the obtained specimens were surgically excised cancer-infiltrated cortical tissue that required removal as part of the surgical treatment. The patients' diagnoses were confirmed based on pathology examination and standardized WHO criteria [71].

Preoperatively, the patients were administered the fluorescent compounds 5-Aminolevulinic acid hydrochloride (5-ALA) (20 mg/kg bodyweight administered orally) and sodium fluorescein (200 mg IV), which allowed the neurosurgeon to visualize the tumor and the areas infiltrated by the tumor [72, 73]. The surgical specimens, ranging between 1-2 cm^3 in volume, were resected from the superficial cortical regions and passed the contrast-enhancing rim of the tumor. The procedure did not impose any constraints on the patients or their surgical treatment. The excised specimens were transferred immediately after resection to a sterile container filled with slicing artificial cerebrospinal fluid (ACSF). The slicing ACSF comprised (in mM): 75 Sucrose, 84 NaCl, 2.5 KCl, 1 NaH_2PO_4, 25 $NaHCO_3$, 25 D-glucose, 0.5 $CaCl_2 \cdot 2H_2O$ and 4 $MgCl_2 \cdot 6H_2O$. The pH was adjusted to 7.3–7.4 using concentrated hydrochloric acid. The osmolality was confirmed to be between 295– 305 mOsm kg^{-1}. The solution was pre-chilled and thoroughly bubbled with carbogen (95% O2, 5% CO2) gas before tissue collection. During transportation, the tissue was kept in a continuously

carbogenated slicing ACSF solution maintained at a constant temperature. The duration of tissue transport from the operating room to the laboratory site ranged from 15 to 30 minutes.

Tissue processing

The tissue processing followed the procedure described in our previous work [69, 74]. The human ex vivo brain slice culture method was developed based on previously established procedures [75-77]. The tissue samples underwent thorough examination to identify the most effective method for blocking and mounting them onto the vibrating microtome platform, Leica 1200S vibratome (Leica Microsystems, Denmark). The samples were sliced perpendicular to the pial surface to preserve dendrite and axon integrity in the GBM-infiltrated region. The tissue slicing procedure was performed in sterile-filtered and chilled ACSF slicing solution. The solution was saturated with carbogen gas to maintain tissue oxygenation throughout the processing steps. Slices of 300 µm thickness were cut and transferred to a carbogenated (95% O2/5% CO2) and tempered (34 °C) slicing ACSF solution to recover for 30 min. The slices were then transferred onto membrane inserts (Millipore) in 6 well plates with 800µL per well of slice culture media of the composition: 8.4 g/L MEM Eagle medium, 20% heat-inactivated horse serum, 30 mM HEPES, 13 mM D-glucose, 15 mM $NaHCO_3$, 1 mM ascorbic acid, 2 mM $MgSO_4 \cdot 7H_2O$, 1 mM $CaCl_2.4H_2O$, 0.5 mM GlutaMAX-I and 1 mg/L insulin, 25 U/mL Penicillin/Streptomycin. The slice culture medium was adjusted to pH 7.2–7.3 by addition of 1 M Tris base. The osmolality was adjusted to 295–305 mOsmoles kg^{-1} by addition of pure H_2O. The tissues were cultured humidified with 5% CO_2 in an incubator at 37°C. The slice culture medium was replenished every one to two days until the experiment was completed. One to three hours after the brain slices were transferred onto cell culture inserts, the brain slices were transduced by direct application of concentrated AAV viral particles over the slice surface for fluorescent labelling. Two days later the slices were transferred onto 1 mm thick slices of 2% w/v GelMA-B or GelMA-F on membrane inserts, or directly onto separate membrane inserts in 6-well plates.

AAV-viral transduction

The adeno-associated virus (AAV) transduction followed the procedure described in our previous work [69, 74]. The AVV vectors were acquired from the University of Zurich Viral Vector Facility. The optimized hGFAP-AAV vector virus (ssAAV5-hGFAP-hHEbl/E-EGFP-bGHp(A)) was used to label astrocyte or glioblastoma cells with fluorescent eGFP. The functional virus titers ranged between $1–3 \times 10^{13}$ units per mL. Human slice cultures were transduced with AAV amplicons by directly applying the concentrated viral stock solutions to the slice surface using a fine micropipette. This was done at least one hour after plating to allow the slice to equilibrate. The virus was carefully spread over the entire slice surface, ensuring that the surface tension of the viral solution was maintained without it spreading onto the membrane insert.

Live/dead imaging

PC12 and eGFP-MSC cells were cultured and maintained as described in the Cell Culture section. After the stated days of culture, the sample wells were gently rinsed with warm growth media. Live/dead solution was prepared by diluting Calcein-AM (2 mM in DMSO) 1:1000 and propidium iodide (PI) (1.5 mM in deionized H_2O) 1:500 in 37 °C cell culture medium without serum and phenol red. The growth medium was removed. 300 µL Live/dead solution was added to each sample well and incubated for 30 minutes at 37 °C and 5% CO_2 protected from light. The live/dead solution was subsequently removed and replaced with cell culture medium without serum or phenol red. Fluorescence imaging was immediately performed using EVOS FL Auto Cell Imaging System (Invitrogen). For Calcein 494nm/517nm (excitation/emission) was used and for PI 535nm/617nm was used.

Immunostaining and fluorescence imaging

After ended culture, samples were fixed in 4% formaldehyde solution for 20 minutes, and subsequently permeabilized in PBS with 2% Triton X-100 for 15 minutes. After blocking in 1% bovine serum albumin (BSA)/PBS (Sigma, A2153) solution for 1 hour at room temperature cells were immunostained with rabbit anti-β-III-tubulin (Abcam ab18207, 1:1000) primary antibody, chicken anti-GFAP (Invitrogen, PA1-10004, 1:1000), and Guinea pig anti-Synaptophysin (Alomone Labs, ANR-013-GP200UL, 1:200) at 4 °C overnight. After washing with PBS, cells were stained with Donkey anti-mouse (Alexa Fluor 594, Abcam, 1:1000), Goat anti-chicken IgY (Alexa Fluor TM 488, Invitrogen, A-11039, 1:500), and goat anti-guinea pig IgG (Alexa Fluor 633, Invitrogen, A-21105, 1:1000) secondary antibody for 1 hour at room temperature. After washing with PBS again, Hoechst 33258 (Life Technologies, 1:10,000) was added for 10 minutes to stain cell nuclei. For brain tissue slices the permeabilization, blocking, staining, and washing steps were performed using Perm/Wash (BD Biosciences, 554723) instead of Triton X-100, BSA, BSA, and PBS, respectively. Fluorescence images were acquired with an EVOS FL Auto Cell Imaging System (Invitrogen).

Cell neurite length was manually traced and evaluated from cell fluorescence images using ImageJ [78] with NeuronJ [79] plugin-software. Neurites longer than the cell body and not extending outside of the field of view were included. The average neurite length is defined as the total neurite length divided by the total neurite number. At least 300 neurites were measured from each condition. The manual tracing was performed blinded to the experimental condition.

Statistics

The data is represented as a mean ± standard deviation. Statistical significance was analyzed using Kruskal-Wallis test with Dunn's test to correct for multiple comparisons using GraphPad Prism software. The values of $*p < 0.05$, $**p < 0.01$, $***p < 0.001$, and $****p<0.0001$ indicates significant difference.

Acknowledgements

We gratefully acknowledge the support of Novo Nordisk Foundation (NNF22OC0080508), Lundbeck Foundation (R400-2022-1232), Carlsberg Foundation (CF19–0300), Marie Skłodowska-Curie grant agreement ENSIGN (101086226) and L4DNANO (101086227) for the support.

References

1. Rauti, R., N. Renous, and B.M. Maoz, *Mimicking the Brain Extracellular Matrix in Vitro: A Review of Current Methodologies and Challenges.* Israel Journal of Chemistry, 2020. **60**(12): p. 1141-1151.
2. Streitberger, K.-J., et al., *Brain Viscoelasticity Alteration in Chronic-Progressive Multiple Sclerosis.* PLOS ONE, 2012. **7**(1): p. e29888.
3. Soria, F.N., et al., *Synucleinopathy alters nanoscale organization and diffusion in the brain extracellular space through hyaluronan remodeling.* Nature Communications, 2020. **11**(1): p. 3440.
4. Hu, Y., et al., *An ECM-Mimicking, Injectable, Viscoelastic Hydrogel for Treatment of Brain Lesions.* Advanced Healthcare Materials, 2023. **12**(1): p. 2201594.
5. Novak, C.B., et al., *Relationships Among Pain Disability, Pain Intensity, Illness Intrusiveness, and Upper Extremity Disability in Patients With Traumatic Peripheral Nerve Injury.* The Journal of Hand Surgery, 2010. **35**(10): p. 1633-1639.
6. Griffin, J.W., et al., *Peripheral Nerve Repair and Reconstruction.* The Journal of Bone & Joint Surgery, 2013. **95**(23): p. 2144-2151.
7. Li, R., et al., *Peripheral Nerve Injuries Treatment: a Systematic Review.* Cell Biochemistry and Biophysics, 2014. **68**(3): p. 449-454.
8. Bell J. H. A., H.J.W., *Next Generation Nerve Guides: Materials, Fabrication, Growth Factors, and Cell Delivery.* Tissue Engineering Part B: Reviews, 2012. **18**(2): p. 116-128.
9. Kornfeld, T., P.M. Vogt, and C. Radtke, *Nerve grafting for peripheral nerve injuries with extended defect sizes.* Wiener Medizinische Wochenschrift (1946), 2019. **169**(9): p. 240-251.
10. Samanta, S., et al., *Bidirectional cell-matrix interaction dictates neuronal network formation in a brain-mimetic 3D scaffold.* Acta Biomaterialia, 2022. **140**: p. 314-323.
11. Kato-Negishi, M., et al., *Millimeter-Sized Neural Building Blocks for 3D Heterogeneous Neural Network Assembly.* Advanced Healthcare Materials, 2013. **2**(12): p. 1564-1570.
12. Bouyer, C., et al., *A Bio-Acoustic Levitational (BAL) Assembly Method for Engineering of Multilayered, 3D Brain-Like Constructs, Using Human Embryonic Stem Cell Derived Neuro-Progenitors.* Advanced Materials, 2016. **28**(1): p. 161-167.
13. Tan, Z., et al., *Cryogenic 3D Printing of Super Soft Hydrogels.* Scientific Reports, 2017. **7**(1): p. 16293.
14. Tang-Schomer, M.D., et al., *Bioengineered functional brain-like cortical tissue.* Proceedings of the National Academy of Sciences, 2014. **111**(38): p. 13811-13816.
15. Tan, H.-Y., H. Cho, and L.P. Lee, *Human mini-brain models.* Nature Biomedical Engineering, 2021. **5**(1): p. 11-25.
16. Chaudhuri, O., et al., *Effects of extracellular matrix viscoelasticity on cellular behaviour.* Nature, 2020. **584**(7822): p. 535-546.
17. Hoffman-Kim, D., J.A. Mitchel, and R.V. Bellamkonda, *Topography, Cell Response, and Nerve Regeneration.* Annual Review of Biomedical Engineering, 2010. **12**(1): p. 203-231.
18. Leclech, C., et al., *Topographical cues control the morphology and dynamics of migrating cortical interneurons.* Biomaterials, 2019. **214**: p. 119194.
19. Leclech, C. and C. Villard, *Cellular and Subcellular Contact Guidance on Microfabricated Substrates.* Frontiers in Bioengineering and Biotechnology, 2020. **8**: p. 551505.
20. Yang, S., et al., *Aligned fibrin/functionalized self-assembling peptide interpenetrating nanofiber hydrogel presenting multi-cues promotes peripheral nerve functional recovery.* Bioactive Materials, 2022. **8**: p. 529-544.
21. Jeffries, E.M. and Y. Wang, *Incorporation of parallel electrospun fibers for improved topographical guidance in 3D nerve guides.* Biofabrication, 2013. **5**(3): p. 035015.
22. Jensen, B.N., et al., *Wireless electromagnetic neural stimulation patch with anisotropic guidance.* npj Flexible Electronics, 2023. **7**(1): p. 1-11.
23. Wang, Y., et al., *An injectable high-conductive bimaterial scaffold for neural stimulation.* Colloids and Surfaces B: Biointerfaces, 2020. **195**: p. 111210.

24. Zhang, Z., et al., *3D anisotropic photocatalytic architectures as bioactive nerve guidance conduits for peripheral neural regeneration.* Biomaterials, 2020. **253**: p. 120108.
25. *In Vitro Assessment of Axonal Growth Using Dorsal Root Ganglia Explants in a Novel Three-Dimensional Collagen Matrix.* Tissue Engineering, 2007. **13**(12): p. 2971-2979.
26. Rao, Z., et al., *Decellularized nerve matrix hydrogel scaffolds with longitudinally oriented and size-tunable microchannels for peripheral nerve regeneration.* Materials Science and Engineering: C, 2021. **120**: p. 111791.
27. Lu, Q., et al., *Nerve Guidance Conduits with Hierarchical Anisotropic Architecture for Peripheral Nerve Regeneration.* Advanced Healthcare Materials, 2021. **10**(14): p. 2100427.
28. Johnson, B.N., et al., *3D Printed Anatomical Nerve Regeneration Pathways.* Advanced Functional Materials, 2015. **25**(39): p. 6205-6217.
29. Jakus, A.E., et al., *Three-Dimensional Printing of High-Content Graphene Scaffolds for Electronic and Biomedical Applications.* ACS Nano, 2015. **9**(4): p. 4636-4648.
30. Rizzo, R., et al., *Optimized Photoclick (Bio)Resins for Fast Volumetric Bioprinting.* Advanced Materials, 2021. **33**(49): p. 2102900.
31. Bernal, P.N., et al., *Volumetric Bioprinting of Complex Living-Tissue Constructs within Seconds.* Advanced Materials, 2019. **31**(42): p. 1904209.
32. Liu, H., et al., *Filamented Light (FLight) Biofabrication of Highly Aligned Tissue-Engineered Constructs.* Advanced Materials, 2022. **34**(45): p. 2204301.
33. Spitzer, N.C., *Electrical activity in early neuronal development.* Nature, 2006. **444**(7120): p. 707-712.
34. Zuo, K.J., et al., *Electrical stimulation to enhance peripheral nerve regeneration: Update in molecular investigations and clinical translation.* Experimental Neurology, 2020. **332**: p. 113397.
35. Javeed, S., et al., *Application of electrical stimulation for peripheral nerve regeneration: Stimulation parameters and future horizons.* Interdisciplinary Neurosurgery, 2021. **24**: p. 101117.
36. Sridharan, A., S.D. Rajan, and J. Muthuswamy, *Long-term changes in the material properties of brain tissue at the implant-tissue interface.* Journal of neural engineering, 2013. **10**(6): p. 066001.
37. Won, S.M., et al., *Wireless and battery-free technologies for neuroengineering.* Nature Biomedical Engineering, 2021. **7**(4): p. 405-423.
38. del Valle, J. and X. Navarro, *Chapter Two - Interfaces with the Peripheral Nerve for the Control of Neuroprostheses*, in *International Review of Neurobiology*, S. Geuna, et al., Editors. 2013, Academic Press. p. 63-83.
39. Frank, J.A., M.-J. Antonini, and P. Anikeeva, *Next-generation interfaces for studying neural function.* Nature Biotechnology, 2019. **37**(9): p. 1013-1023.
40. Choi, Y.S., et al., *Fully implantable and bioresorbable cardiac pacemakers without leads or batteries.* Nature Biotechnology, 2021. **39**(10): p. 1228-1238.
41. Koo, J., et al., *Wireless bioresorbable electronic system enables sustained nonpharmacological neuroregenerative therapy.* Nature Medicine, 2018. **24**(12): p. 1830-1836.
42. Young, A.T., O.C. White, and M.A. Daniele, *Rheological Properties of Coordinated Physical Gelation and Chemical Crosslinking in Gelatin Methacryloyl (GelMA) Hydrogels.* Macromolecular Bioscience, 2020. **20**(12): p. 2000183.
43. Mondrinos, M.J., et al., *Surface-directed engineering of tissue anisotropy in microphysiological models of musculoskeletal tissue.* Science Advances, 2021. **7**(11): p. eabe9446.
44. Tsai, H.-F., et al., *Uniform electric field generation in circular multi-well culture plates using polymeric inserts.* Scientific Reports, 2016. **6**(1): p. 26222.
45. Chaparro, C.V., et al., *Considerations on electrical impedance measurements of electrolyte solutions in a four-electrode cell.* Journal of Physics: Conference Series, 2016. **687**(1): p. 012101.
46. Xue, W., et al., *Anisotropic scaffolds for peripheral nerve and spinal cord regeneration.* Bioactive Materials, 2021. **6**(11): p. 4141-4160.
47. Shahidi, S., et al., *A tuned gelatin methacryloyl (GelMA) hydrogel facilitates myelination of dorsal root ganglia neurons in vitro.* Materials Science and Engineering: C, 2021. **126**: p. 112131.

48. Repić, T., et al., *Characterization of dorsal root ganglion neurons cultured on silicon micro-pillar substrates.* Scientific Reports, 2016. **6**(1): p. 39560.
49. Nelson, D.W., et al., *Multivariate analysis reveals topography dependent relationships amongst neurite morphological features from dorsal root ganglia neurons.* J Neural Eng, 2022. **19**(3).
50. M.F, G., et al., *Peripheral Nerve Injury: Principles for Repair and Regeneration.* The Open Orthopaedics Journal, 2014. **8**(1): p. 199-203.
51. Lee, J.I., et al., *Purposeful Misalignment of Severed Nerve Stumps in a Standardized Transection Model Reveals Persistent Functional Deficit With Aberrant Neurofilament Distribution.* Military Medicine, 2021. **186**(Supplement_1): p. 696-703.
52. Lenoir, S., et al., *Recreating mouse cortico-hippocampal neuronal circuit in microfluidic devices to study BDNF axonal transport upon glucocorticoid treatment.* STAR Protocols, 2021. **2**(1): p. 100382.
53. Bruno, G., et al., *Microfluidic Multielectrode Arrays for Spatially Localized Drug Delivery and Electrical Recordings of Primary Neuronal Cultures.* Frontiers in Bioengineering and Biotechnology, 2020. **8**.
54. Yang, Y., et al., *Simulation and fabrication of in vitro microfluidic microelectrode array chip for patterned culture and electrophysiological detection of neurons.* Nanotechnology and Precision Engineering, 2024. **7**(2).
55. Harberts, J., et al., *Toward Brain-on-a-Chip: Human Induced Pluripotent Stem Cell-Derived Guided Neuronal Networks in Tailor-Made 3D Nanoprinted Microscaffolds.* ACS Nano, 2020. **14**(10): p. 13091-13102.
56. Bonfanti, L. and P. Peretto, *Adult neurogenesis in mammals – a theme with many variations.* European Journal of Neuroscience, 2011. **34**(6): p. 930-950.
57. Li, X., et al., *Around 90° Contact Angle of Dish Surface Is a Key Factor in Achieving Spontaneous Spheroid Formation.* Tissue Engineering Part C: Methods, 2018. **24**(10): p. 578-584.
58. Joseph, G., et al., *Effects of Surface Chemistry Interaction on Primary Neural Stem Cell Neurosphere Responses.* ACS Omega, 2021. **6**(30): p. 19901-19910.
59. Sun, Y., et al., *Surface Coating as a Key Parameter in Engineering Neuronal Network Structures In Vitro.* Biointerphases, 2012. **7**(1): p. 29.
60. Tang, Y., et al., *Patch method for culture of primary hippocampal neurons.* Microelectronic Engineering, 2017. **175**: p. 61-66.
61. Bansal, M., et al., *Patternable Gelatin Methacrylate/PEDOT/Polystyrene Sulfonate Microelectrode Coatings for Neuronal Recording.* ACS Biomaterials Science & Engineering, 2022. **8**(9): p. 3933-3943.
62. Hörberg, C.J., et al., *Spontaneous Cell Cluster Formation in Human iPSC-Derived Neuronal Spheroid Networks Influences Network Activity.* eNeuro, 2022. **9**(5).
63. Khan, J., et al., *Neurosphere Development from Hippocampal and Cortical Embryonic Mixed Primary Neuron Culture: A Potential Platform for Screening Neurochemical Modulator.* ACS Chemical Neuroscience, 2018. **9**(11): p. 2870-2878.
64. García-Parra, P., et al., *A neural extracellular matrix-based method for in vitrohippocampal neuron culture and dopaminergic differentiation of neural stem cells.* BMC Neuroscience, 2013. **14**(1): p. 48.
65. Antonova, O.Y., et al., *Rapid Generation of Neurospheres from Hippocampal Neurons Using Extracellular-Matrix-Mimetic Scaffolds.* ACS Chemical Neuroscience, 2021. **12**(15): p. 2838-2850.
66. Eskandari, F., et al., *Structural Anisotropy vs. Mechanical Anisotropy: The Contribution of Axonal Fibers to the Material Properties of Brain White Matter.* Annals of Biomedical Engineering, 2021. **49**(3): p. 991-999.
67. Vaegter, C.B., et al., *Sortilin associates with Trk receptors to enhance anterograde transport and neurotrophin signaling.* Nature Neuroscience, 2011. **14**(1): p. 54-61.
68. Sun, C., et al., *The prevalence and specificity of local protein synthesis during neuronal synaptic plasticity.* Science Advances, 2021. **7**(38): p. eabj0790.
69. Tong, T., et al., *Glioblastoma cells imitate neuronal excitability in humans.* bioRxiv, 2024: p. 2024.01.08.574637.

70. Association, W.M., *Declaration of Helsinki. Ethical Principles for Medical Research Involving Human Subjects.* Jahrbuch für Wissenschaft Und Ethik, 2009. **14**(1): p. 233-238.
71. Louis, D.N., et al., *The 2021 WHO classification of tumors of the central nervous system: a summary.* Neuro-oncology, 2021. **23**(8): p. 1231-1251.
72. Hansen, R.W., et al., *Comparison of 5-aminolevulinic acid and sodium fluorescein for intraoperative tumor visualization in patients with high-grade gliomas: a single-center retrospective study.* Journal of Neurosurgery, 2019. **133**(5): p. 1324-1331.
73. Ahrens, L.C., et al., *Effect of 5-aminolevulinic acid and sodium fluorescein on the extent of resection in high-grade gliomas and brain metastasis.* Cancers, 2022. **14**(3): p. 617.
74. Kurmasheva, N., et al., *Octyl itaconate enhances VSVΔ51 oncolytic virotherapy by multitarget inhibition of antiviral and inflammatory pathways.* Nat Commun, 2024. **15**(1): p. 4096.
75. Ting, J.T., et al., *A robust ex vivo experimental platform for molecular-genetic dissection of adult human neocortical cell types and circuits.* Scientific reports, 2018. **8**(1): p. 8407.
76. Louth, E.L., et al., *Dopaminergic neuromodulation of spike timing dependent plasticity in mature adult rodent and human cortical neurons.* Frontiers in Cellular Neuroscience, 2021. **15**: p. 668980.
77. Lee, B.R., et al., *Signature morphoelectric properties of diverse GABAergic interneurons in the human neocortex.* Science, 2023. **382**(6667): p. eadf6484.
78. Schneider, C.A., W.S. Rasband, and K.W. Eliceiri, *NIH Image to ImageJ: 25 years of image analysis.* Nature Methods, 2012. **9**(7): p. 671-675.
79. Meijering, E., et al., *Design and validation of a tool for neurite tracing and analysis in fluorescence microscopy images.* Cytometry. Part A: The Journal of the International Society for Analytical Cytology, 2004. **58**(2): p. 167-176.

Supplementary information

Bjarke Nørrehvedde Jensen[1], Christoph Müller[1], Tong Tong[2,3], Cecillie Linneberg Matthiesen[1], Dror Seliktar[4], Mingdong Dong[5], Anders Rosendal Korshøj[2,3], Menglin Chen[1,5*]

[1] *Department of Biological and Chemical Engineering, Aarhus University, Aarhus, Denmark*

[2] *Department of Neurosurgery, Aarhus University Hospital, Palle Juul-Jensens Boulevard 165, 11 8200 Aarhus N, Denmark*

[3] *Department of Clinical Medicine, Aarhus University, Palle Juul-Jensens Boulevard 99, 8200 13 Aarhus N, Denmark*

[4] *Faculty of Biomedical Engineering, Technion – Israel Institute of Technology, Haifa 32000, Israel*

[5] *Interdisciplinary Nanoscience Center, Aarhus University, Aarhus, Denmark*

[*] *Corresponding author; Menglin@BCE.au.dk*

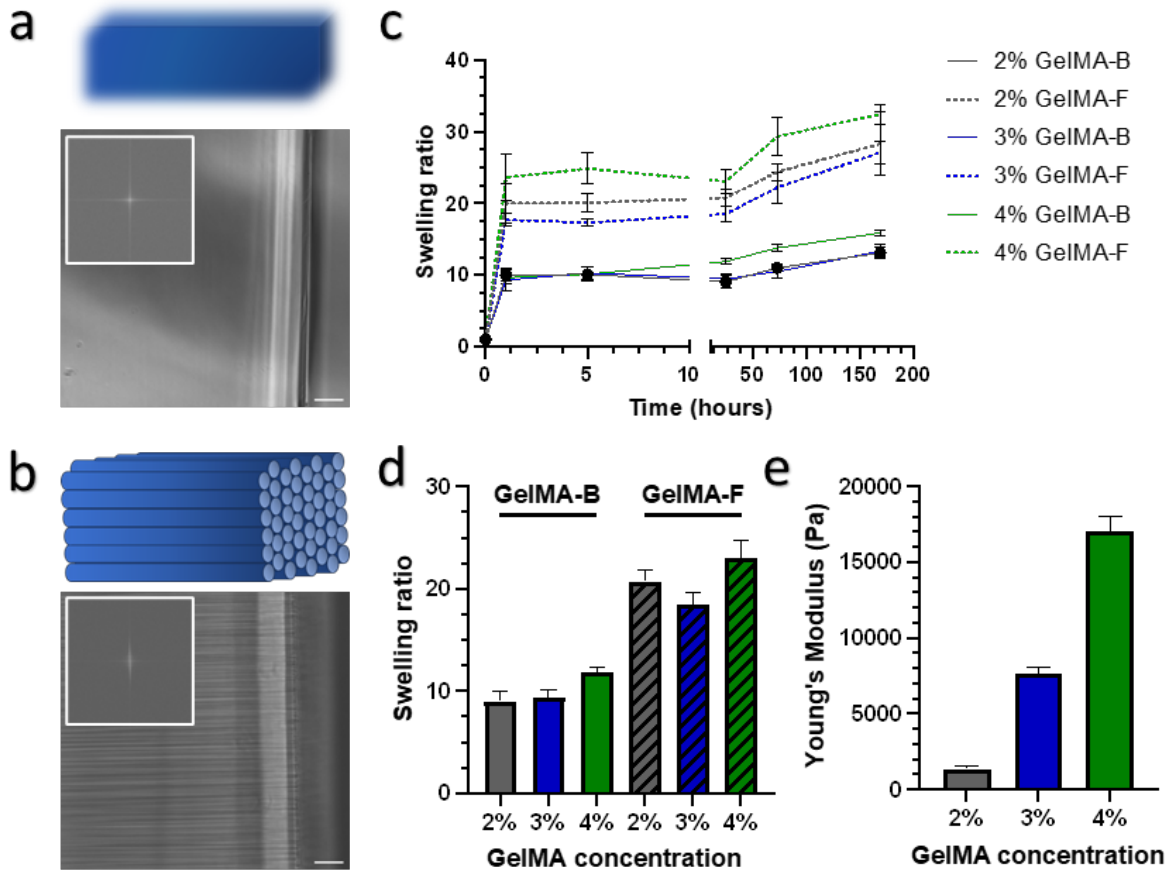

Figure S1 – Mechanical characterization of GelMA. ***a)*** *Schematic and brightfield image with FFT insert of 4% w/v GelMA-B.* ***b)*** *Schematic and brightfield image with FTT insert of 4% w/v GelMA-F.* ***c-d)*** *Swelling ratios of GelMA-B and GelMA-F.* ***e)*** *Young's modulus of GelMA-B calculated from mechanical compression measurements. Scalebars: 100 µm.*

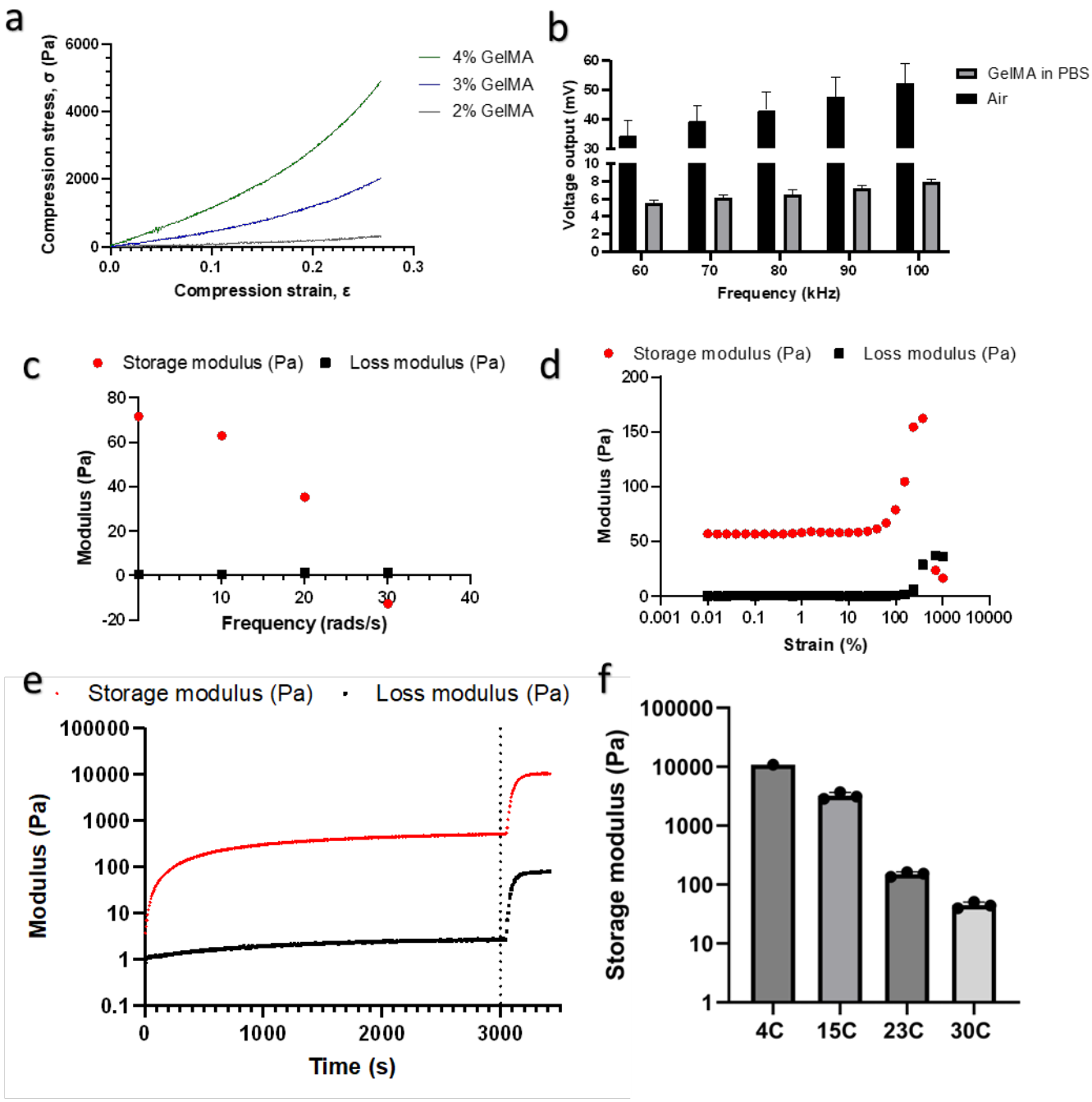

Figure S2 – Rheological measurements of GelMA. ***a)*** Compression stress-strain curves of GelMA. ***b)*** *Induced voltage in neural stimulation patch.* ***c)*** *Frequency test of 4% w/v GelMA at 23 °C.* ***d)*** *Stain test of 4% w/v GelMA at 23 °C.* ***e)*** *Physical gelation of GelMA (before dotted line) at 4 °C followed by light mediated chemical crosslinking (after dotted line).* ***f)*** *Storage modulus of physical gelation of 4% w/v GelMA at various temperatures followed by light mediated chemical crosslinking.*

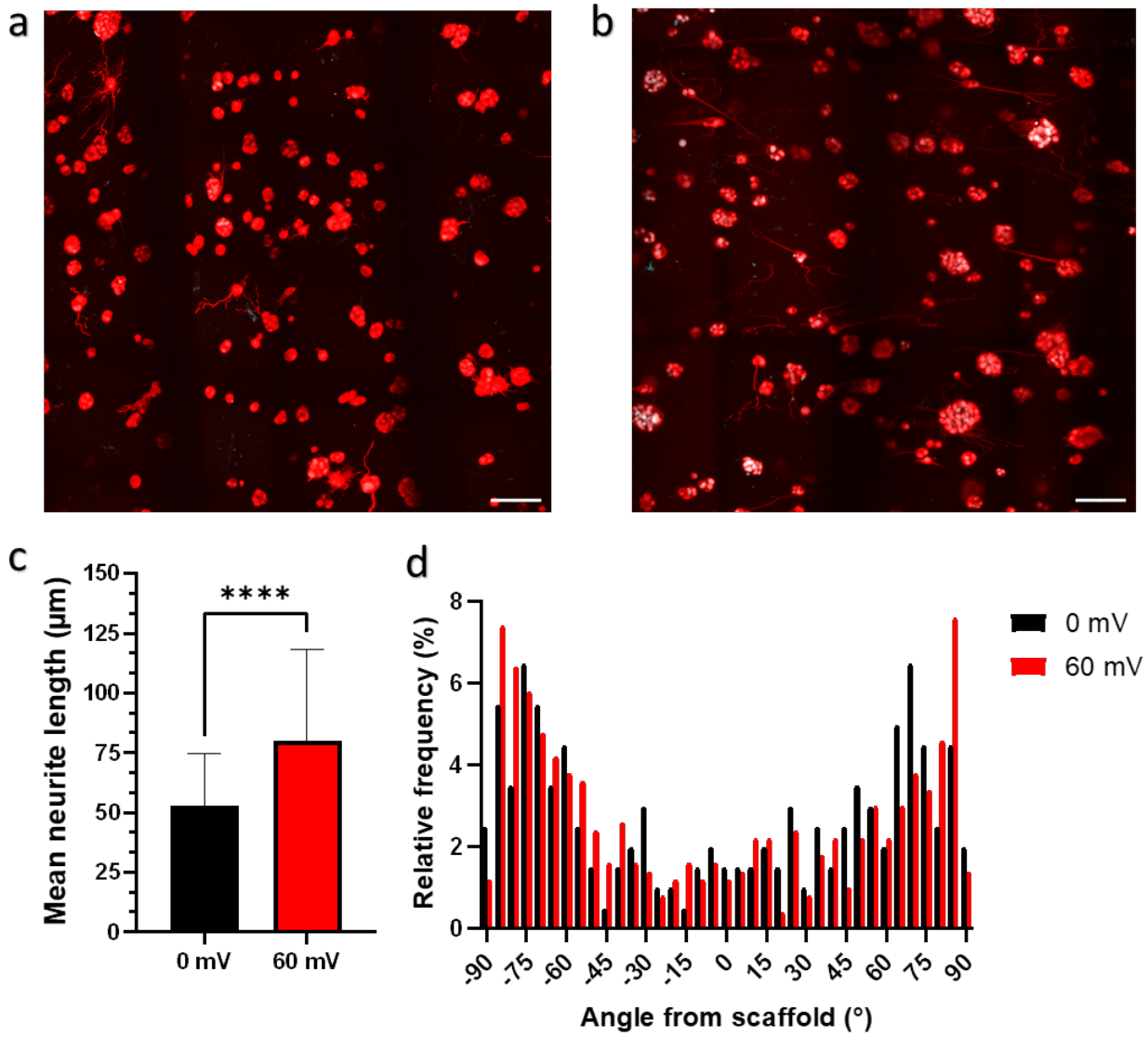

Figure S3 – PC12 neurite outgrowth in GelMA with EM stimulation. *PC12 in 4% GelMA (RT) after 5 days of NGF differentiation with a) 0 mV EM stimulation, and b) 60 mV EM stimulation. c) Mean neurite outgrowth of PC12 cells in GelMA with EM stimulation. d) Directionality of PC12 neurites in GelMA with EM stimulation after 5 days of NGF differentiation. Scalebar = 100 µm.*

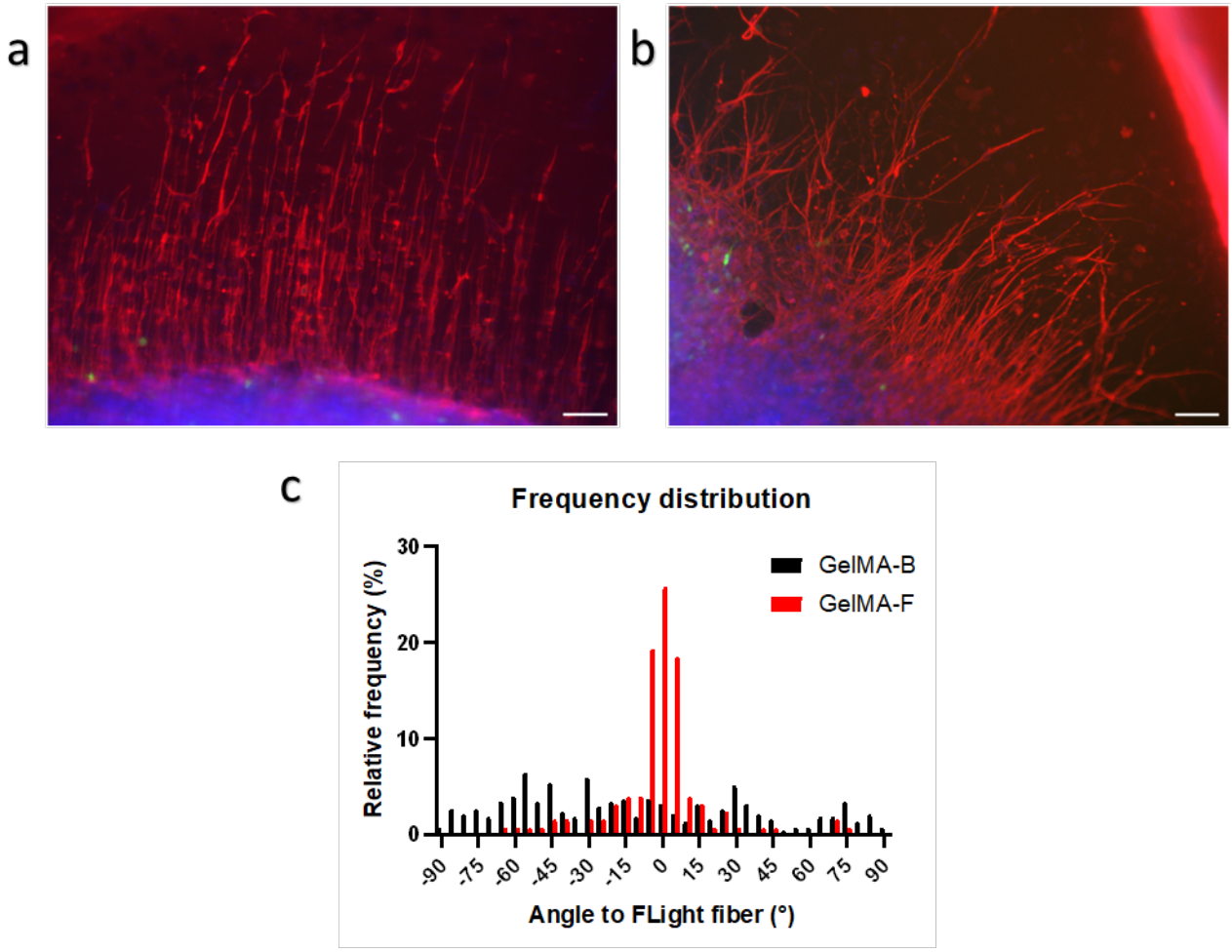

Figure S4 – Human brain tissue on GelMA-B and GelMA-F. *Human brain tissue after 7 days of culture on 2% w/v* ***a)*** *GelMA-F and* ***b)*** *GelMA-B.* ***c)*** *Outgrowth directionality analysis from* ***a)*** *and* ***b)*** *samples. Blue = Hoechst, red = β-III-tubulin, green = glioblastoma. Scalebar* ***a-b*** *= 100 µm.*

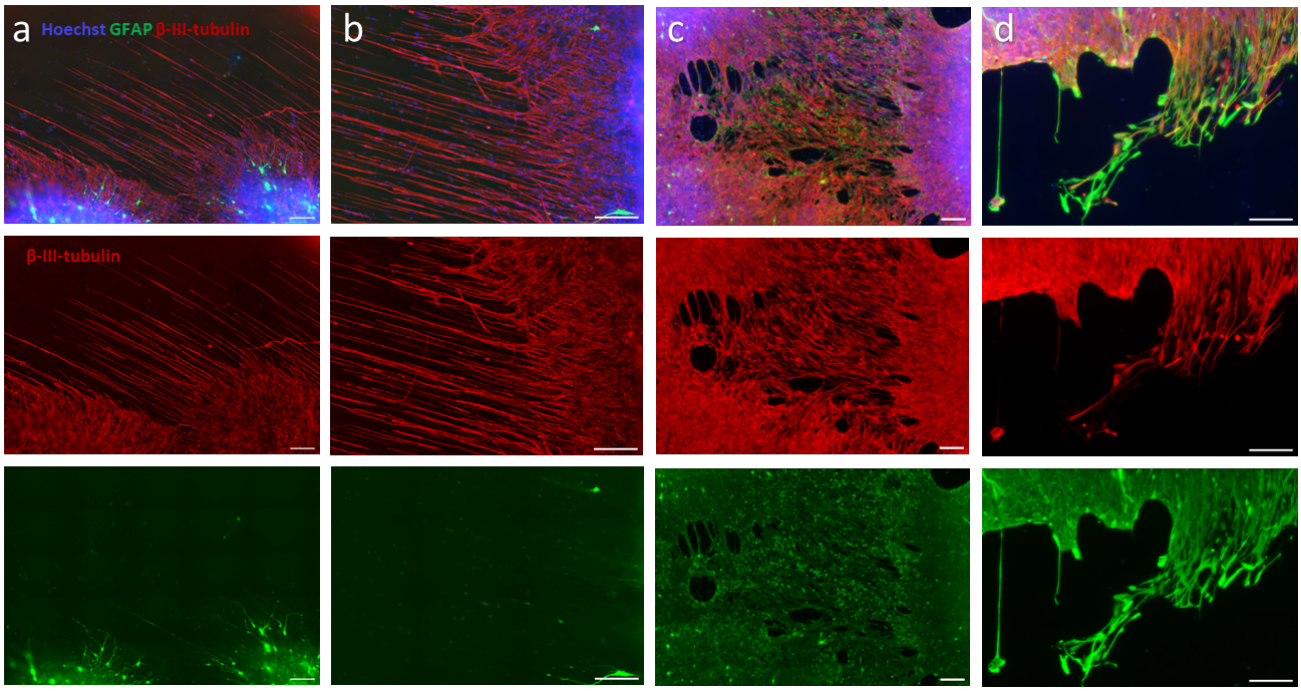

Figure S5 – Human brain tissue on membrane well-insert and GelMA-F. *Human brain tissue after 21 days of culture on 2% w/v* ***a-b)*** *GelMA-F and* ***c-d)*** *membrane well-insert post-stained for GFAP (green). Blue = Hoechst, red = β-III-tubulin, green = glioblastoma/GFAP. Scalebar* ***a-d*** *= 200 µm.*